Applied Catalysis B: Environmental 154–155 (2014) 161–170

Contents lists available at ScienceDirect

Applied Catalysis B: Environmental

journal homepage: www.elsevier.com/locate/apcatb

Bifunctional Cu/H-ZSM-5 zeolite with hierarchical porosity for hydrocarbon abatement under cold-start conditions

B. Puértolas[a], L. García-Andújar[a], T. García[a], M.V. Navarro[a,*], S. Mitchell[b], J. Pérez-Ramírez[b]

[a] Instituto de Carboquímica (ICB-CSIC), C/Miguel Luesma Castán, 50018 Zaragoza, Spain
[b] Institute for Chemical and Bioengineering, Department of Chemistry and Applied Biosciences, ETH Zurich, Vladimir-Prelog-Weg 1, CH-8093 Zurich, Switzerland

ARTICLE INFO

Article history:
Received 2 December 2013
Received in revised form 3 February 2014
Accepted 8 February 2014
Available online 18 February 2014

Keywords:
Cold-start vehicle emissions
Cu/H-ZSM-5
Hierarchical zeolite
Bifunctional catalysis

ABSTRACT

A key target to reduce current hydrocarbon emissions from vehicular exhaust is to improve their abatement under cold-start conditions. Here, we demonstrate the exceptional properties of a hierarchical Cu/H-ZSM-5 zeolite-based system as a catalytic trap. The largely increased external surface area coupled with the preserved intrinsic properties attainable upon alkaline treatment and subsequent acid washing of a conventional ZSM-5 zeolite enable an improved dispersion of copper species in the hierarchical counterpart. The impact of post-synthetic modification on the preparation of copper-containing ZSM-5 is clearly revealed by XRD, N_2 sorption, FTIR, NH_3-TPD, TEM, SEM, and HAADF-STEM. By providing stronger adsorption sites, the introduction of copper species improves the retention of propene and toluene with respect to the protonic zeolites, and enables their further conversion to carbon dioxide and water rather than their emission in the exhaust. The equivalent adsorption capacity and improved oxidation activity and lower susceptibility to deactivation exhibited by the hierarchical Cu/H-ZSM-5 catalyst vis-a-vis its conventional counterpart yield a superior bifunctional catalyst able of reach full hydrocarbon conversion under realistic operating conditions.

1. Introduction

Air pollution poses a major environmental concern worldwide. In metropolitan areas, motor vehicle exhaust contributes a major source of contaminants. With current three-way catalysts (TWCs), a recognized challenge in preventing these emissions is the lack of treatment capacity of hydrocarbons (HC) under cold-start conditions. In a standard driving cycle, i.e. a New European Drive cycle (NEDC) for a 2,0 l diesel engine [1], the catalyst takes ca. 1–2 min to reach its operating temperature of between 200 and 300 °C. For gasoline engines, this time is very variable and depends on the engine operation conditions. Of the scarce examples in the literature, Choi et al. [2] observed that the catalyst of a gasoline engine reached 500 °C in 30 s for a 2,0 l SULEV. During this time, about 50–80% of unburned HCs are emitted [3]. To curb these emissions, the incorporation of an inorganic nanoporous material to act as a HC trap prior to the TWC, is one of the most promising solutions. The adsorbent must be able to capture the HCs at low temperatures and not to release them before reaching the optimal catalyst operating temperature. This strategy could be more efficient, compared with other methods such as exhaust burner or the electrically-heated catalyst [4]. However, in terms of efficiency, the comparison between the HC trap and the close-coupled catalyst strategies is not straightforward. As replacing a close-coupled catalyst with an underfloor HC trap could imply a long delay in pollutant light-off for HC, CO and NO_x, the success will depend on finding an optimal configuration together with the TWC. A HC trap with catalytic properties placed after the TWC could also be a possibility. Zeolites are often considered as HC trap materials due to their stability under a variety of conditions [5,6]. Different zeolites and zeotypes, with varying pore dimensionality and pore network connectivity, have been studied as adsorbents for HC emission control during the cold-start period [7–9]. However, none of the reported materials have demonstrated the necessary characteristics of a HC trap under very demanding operational conditions. It has been found that while heavier exhaust HCs (e.g. aromatics) are adequately trapped, lighter HC components in the exhaust, such as propene, are released before the TWC has reached its light-off temperature [8]. In this sense, a priority goal is to find an adsorbent that fulfills this requirement. Furthermore, the treatment of alkane species may prove a challenge

* Corresponding author. Tel.: +34 976 733977; fax: +34 976 733318.
E-mail address: navarro@icb.csic.es (M.V. Navarro).

http://dx.doi.org/10.1016/j.apcatb.2014.02.013
0926-3373/

as they are not strongly chemisorbed by the Brønsted acid or copper sites [10]. These species must be dealt with by oxidation over a catalyst above 300 °C.

Previous results showed that ZSM-5 zeolites (MFI-type framework) could be a promising material as a HC trap [3,11–17]. It has been observed that propene retention under cold-start conditions could be improved by ion exchange of the zeolite with transition metals, such as copper, in order to create selective adsorption points for light HCs [18]. A direct correlation was observed between the degree of copper exchange and the trapping efficiency [10,19–23]. If the loading was too high, however, large copper oxide nanoparticles formed on the external surface of the zeolite instead of increasing the amount of copper in ion exchange sites. Although these nanoparticles enhanced the oxidation of the HCs upon reaching the desorption temperature, higher copper loadings appeared detrimental for their initial function as a HC trap. Both propene and toluene molecules (two of the primary HC pollutants) were desorbed at lower temperatures than those required for optimal operation [19].

It is worth mentioning that Cu/H-ZSM-5 has shown promising activity and selectivity in several automotive applications, as the direct decomposition of NO and the selective catalytic reduction of NH_3 and HCs. However, their application has been limited by a lack of hydrothermal stability of the zeolite and by sintering of the copper species [24–26], which have been evidenced at operating temperatures between 600 and 800 °C. The extent of sintering is known to increase with temperature, aging time, and in the presence of steam, and it may pose a challenge during cyclic operation as a cold-start trap. Furthermore, since higher temperatures (up to 700 °C) are expected in front of the TWC than after, differences in the severity of sintering are expected to depend on the positioning of the HC trap in the catalytic converter.

A recent study showed that the sintering of cobalt catalysts could be suppressed when supported on hierarchical zeolites, offering a greatly increased external surface area coupled with the largely preserved crystallinity and acidic properties of conventional zeolites [27–29], thereby improving their stability in Fischer-Tropsch synthesis [30]. The application of hierarchical zeolites could potentially also lead to a more efficient catalytic trap by enhancing (i) the accessibility to copper species in ion-exchange positions, (ii) the dispersion of copper oxide nanoparticles, and ultimately (iii) the HC abatement under cold-start conditions. Accordingly, this manuscript investigates the impact of hierarchical structuring on the performance of copper-loaded ZSM-5 zeolites in cold-start tests (CST) representative of standard gasoline engine emissions. Since in practice the gas-hourly space velocity (GHSV) may vary between 10 and 100 K h^{-1} [31], the HC traps are evaluated at 60 K h^{-1}, presenting more demanding experimental conditions than in previous works [18,19]. The traps are fully characterized before and after application in three CST cycles to assess their stability under the operating conditions.

2. Experimental

2.1. Preparation of Cu-loaded hierarchical zeolites

A commercial ZSM-5 zeolite (CBV 8014, Zeolyst International, nominal Si/Al ratio = 40, NH_4-form) was converted to the protonic form by calcination at 450 °C for 6 h in static air (ramp rate = 5 °C min^{-1}). Hierarchical ZSM-5 was prepared by desilication in stirred aqueous sodium hydroxide (≥98% Sigma Aldrich) solution (0, 2 M, 65 °C, 30 min, 30 cm^3 per gram of zeolite) followed by sequential treatment in aqueous hydrochloric acid (37 wt% Sigma Aldrich) solution (0, 1 M, 65 °C, 6 h, 100 cm^3 per gram of zeolite) to restore a similar bulk Si/Al ratio to that of the conventional zeolite [32]. The slurries resulting from each step were quenched in ice-water, filtered, and the isolated solids washed extensively with deionized water and dried at 105 °C for 13 h. The hierarchical sample was converted into the H-form by two consecutive ion exchanges in aqueous ammonium nitrate (99,8% Fisher Scientific) solution (1 M, 80 °C, 24 h, 12 cm^3 per gram of zeolite) followed by calcination as described above. Copper introduction was achieved by treating the zeolites (3 g) in stirred aqueous solutions of copper nitrate (99% Sigma Aldrich) (100 mM, 16.6 cm^3 per gram of zeolite). The pH of the solution was adjusted to 6 by addition of ammonium hydroxide solution (1 M) prior to heating under reflux at 100 °C for 24 h. Subsequently, the copper-containing samples were filtered, washed, dried as above, and finally calcined at 550 °C for 4 h (ramp rate = 1 °C min^{-1}). The conventional and hierarchical ZSM-5 zeolites are coded H-ZSM-5 and mesoH-ZSM-5, respectively, and the copper-containing catalysts are coded Cu/H-ZSM-5 and Cu/mesoH-ZSM-5.

2.2. Characterization

X-ray diffraction (XRD) patterns were measured with a Bruker D8 Advance series II diffractometer using monochromatic Cu Kα radiation (λ = 0,1541 nm). Data were collected in the 2θ range from 3° to 40° using a scanning rate of 1° min^{-1}. N_2 isotherms at −196 °C were measured in a Quantachrome Autosorb 1 gas adsorption analyzer. Prior to the adsorption measurements, the samples were outgassed in situ under vacuum (4 mbar) at 250 °C for 4 h. The total surface area (S_{BET}) was estimated using the BET method, the micropore volume (V_{MICRO}) and mesopore surface area (S_{MESO}) were determined by applying the *t*-plot method, the mesopore size distribution was calculated by applying the BJH method to the desorption branch of the isotherm, and the mesopore volume (V_{MESO}) was estimated as: $V_{MESO} = V_{P/P0=0.99} - V_{MICRO}$. The copper content in the solids was measured by inductively coupled plasma-optical emission spectroscopy (ICP-OES), in a Jobin Ybon 2000 instrument. Secondary and back-scattered electron images (SEM) were acquired using a Zeiss Gemini 1530 FEG microscope operated at 5 kV (SE) or 10 kV (BSE). Transmission electron microscopy (TEM) and high-angle annular dark field scanning (HAADF-STEM) images were acquired using a FEI Technai F30 microscope operated at 300 kV. The samples were supported on holey carbon coated copper grids by dry dispersion. Temperature-programmed desorption of ammonia (NH_3-TPD) was measured by using a Micromeritics Pulse Chemisorb 2700 instrument equipped with a thermal conductivity detector. The catalysts (0.2 g) were degassed under Ar flow at 500 °C for 6 h followed by saturation at 50 °C using 30 cm^3 STP min^{-1} flow of 5% (v/v) NH_3 in Ar. The gas mixture was then switched back to Ar and the sample was purged at 50 °C for 30 min. NH_3-TPD profiles were subsequently recorded under 30 cm^3 STP min^{-1} He flow, from 50 to 600 °C using a ramp rate of 5 °C min^{-1}.

Infrared spectroscopy was performed using a Thermo Nicolet 5700 spectrometer equipped with a SpectraTech Collector II diffuse reflectance accessory and a high-temperature cell. Prior to the measurement, the sample was dried at 300 °C in N_2 flow (60 cm^3 min^{-1}) for 120 min. Spectra were recorded in the range of 650–4000 cm^{-1} with a nominal resolution of 4 cm^{-1} and co-addition of 200 scans after reducing the temperature to 200 °C. The amount of coke formed during the CST was determined by thermogravimetric analysis (TGA). The samples were heated to 900 °C at a rate of 80 °C min^{-1} under flowing air (250 ml min^{-1}), and the weight loss measured between 200 and 900 °C was averaged over three independent measurements.

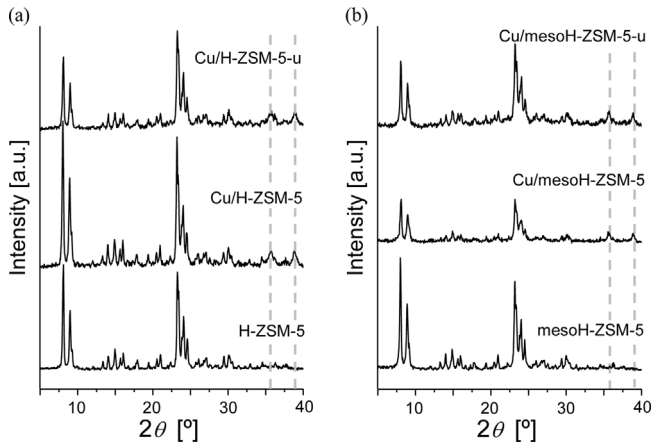

Fig. 1. XRD patterns of the as-synthesized microporous (a) and hierarchical (b) HC traps, and following three CST cycles (designated-u). Marked reflections at $2\theta = 36^\circ$ and 39° correspond to monoclinic CuO.

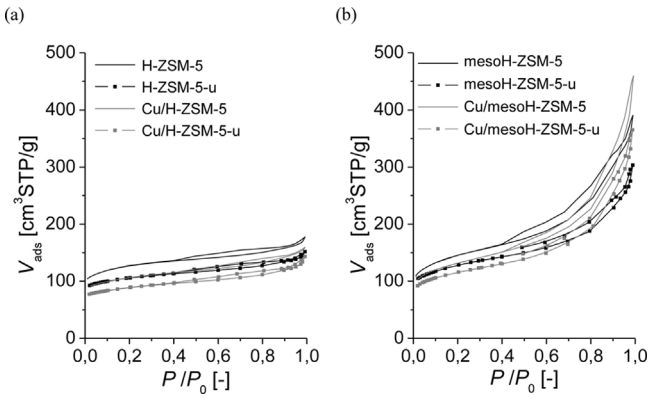

Fig. 2. Nitrogen isotherms at 196 °C of the as-synthesized microporous (a) and hierarchical (b) HC traps, and following three CST cycles (designated-u).

2.3. Simulated cold-start tests

CST experiments were carried out in a fixed-bed reactor (ID = 0.52 cm; 0,10 g of sample) under conditions that closely mimic the automotive "cold start". Prior to each test the zeolite was pretreated *in situ* at 600 °C for 30 min in a flow of argon. In the course of the simulated CSTs, the reactor temperature was increased from 30 to 600 °C at 50 °C min^{-1}, and held at this temperature for a further 30 min. The temperature was measured by a thermocouple located at the top of the catalyst bed. The inlet gas composition used for HC adsorption-desorption experiments was 0,010% (v/v) propene, 0,0087% (v/v) toluene, 1% (v/v) oxygen, 10% (v/v) water in argon leading to a total flow of 100 cm^3 STP min^{-1} and a GHSV of 60 K h^{-1}. According to the literature [33–35], the HC concentration in real exhaust during the cold start period ranges between 100 and 500 ppmv, and thus our value of 200 ppmv is a realistic approximation. The oxygen concentration (1% v/v) was chosen to be representative of standard gasoline engine emissions, in which the values vary between 0,2% and 2% (v/v) [36]. Moreover, the tests were defined to enable proper evaluation of the optimum light-off temperature of the three-way catalysts [37]. Aliquots of the outlet stream were analyzed on line using a quadrupole spectrometer (Omnistar, Pfeiffer Vacuum). The following masses were monitored: $m/z = 40$ for argon, 42 for propene, 91 for toluene, 32 for oxygen and 18 for water; m/z = 55 and 56, related to oligomer formation [17,38,39] and $m/z = 44$ and $m/z = 28$ related to CO_2 formation and CO formation, respectively after HC total oxidation, were also followed during the experiment. Finally, three consecutive CSTs were performed once the reactor was cooled down to assess the reusability of the HC traps. Carbon balances were closed in all the experiments over Cu-loaded hierarchical zeolites ($100 \pm 3\%$), whereas some deviation, observed over the protonic zeolites, is ascribed to oligomer and/or coke formation. In the case of the Cu-loaded conventional ZSM-5, it could also be attributed to the retarded desorption of HC from the structure.

3. Results

3.1. Catalyst properties

The phase purity and crystallinity of the samples before and after application as cold-start HC traps was verified by XRD. Sharp reflections corresponding to the MFI structure [40] were identified in all cases (see Fig. 1). The slightly reduced reflection intensities observed for hierarchical zeolites is as expected following the post-synthetic introduction of intracrystalline mesopores. Additionally, reflections at 36° and 39° in the copper-containing samples, which were more prominent in Cu/H-ZSM-5 than Cu/mesoH-ZSM-5, evidenced the formation of monoclinic CuO (ICSD PDF-number: 01-073-6023 45-937). The segregation of CuO species on ZSM-5 zeolites has been previously observed at high copper loadings [41], and the weaker reflections observed for the hierarchical sample suggest an improved dispersion of copper oxide nanoparticles. Following application in the CSTs, the CuO reflections in the hierarchical material appeared slightly more distinct. However, it was not possible to distinguish differences in the dispersion by application of the Scherrer equation, which indicated an average crystal size of ca. 20 nm in all samples. It should be noted that a reliable analysis of changes in the size of the CuO crystals by XRD is hindered by peak broadening due to the presence of the crystalline zeolite support in addition to instrumental broadening, meaning that smaller crystals may not be detected and high errors may result (>20%).

The copper loading and porous properties of the samples are compiled in Table 1. Analysis by means of ICP-OES revealed a comparable copper content in the conventional and hierarchical zeolites of 77 and 8„6 wt%, respectively, which remained unchanged after use. These loadings are higher than the amount theoretically required to fully occupy all ion exchange sites (ca. 1 wt%), which implies that the remaining copper is randomly deposited over the zeolite particles. As seen in Fig. 2, the conventional H-ZSM-5 exhibited a typical type I isotherm with a limited uptake of N_2 at higher relative pressures. A similar N_2 isotherm was found after copper exchange, Cu/H-ZSM-5, although the micropore volume and mesopore surface area were slightly diminished following the metal introduction. The formation of mesopores upon post-synthetic modification of the conventional zeolite was clearly visible from the types I–IV N_2 isotherms of the hierarchical zeolites shown in Fig. 2 [42]. The increased uptake at high relative pressures ($p/p_0 > 0,5$) corresponded to the filling of the generated mesopores. Analysis of the pore size distribution indicated that mesopores of 12 nm average diameter were developed. This led to a significant increase in mesoporosity in terms of mesopore volume (by 0,43 cm^3 g^{-1}) and mesopore surface area (by 230 cm^3 g^{-1}), that was almost entirely preserved after copper introduction. Following three CST cycles, a slight drop in micropore volume was observed in all cases except for Cu/mesoH-ZSM-5, and a moderate reduction in mesopore surface area (Table 1). The latter could be related to coke deposition, which was evidenced over both the protonic zeolites (ca. 5,2 wt%) and over Cu/H-ZSM-5 (ca. 1.1 wt%) (see Fig. 3). In the case of the copper-loaded zeolites, this could also reflect some sintering of the CuO nanoparticles. Moreover, the higher temperature reached in the CST (600 °C) than during the catalyst preparation

Table 1
Characterization data of the as-prepared HC traps, and after use in three consecutive CSTs.

Sample	Cu content[a] [wt%]	S_{BET}[b] [$m^2\ g^{-1}$]		S_{MESO}[c] [$m^2\ g^{-1}$]		V_{MICRO}[c] [$cm^3\ g^{-1}$]		V_{MESO}[d] [$cm^3\ g^{-1}$]	
	Fresh	Fresh	Used	Fresh	Used	Fresh	Used	Fresh	Used
H-ZSM-5	–	469	392	58	36	0,18	0,16	0,10	0,07
Cu/H-ZSM-5	7,7	392	330	43	43	0,14	0,13	0,11	0,09
mesoH-ZSM-5	–	528	464	284	153	0,10	0,09	0,51	0,38
Cu/mesoH-ZSM-5	8,6	472	421	238	178	0,09	0,09	0,63	0,47

[a] Measured by ICP-OES.
[b] BET method.
[c] *t*-plot method.
[d] $V_{MESO} = V_{P/P0=0,99} - V_{MICRO}$.

(550 °C) can also be the origin of the decreased surface area after use.

Fig. 4 shows representative FEG-SEM micrographs of the conventional and hierarchical zeolites. While both zeolites exhibited comparable particle sizes and morphology, certain differences could be pointed out. Secondary electron (SE) images of the conventional sample revealed some particles of distinct rod-like morphology located at the external surface of the larger zeolite crystals, which could be related to the copper oxide phase detected by XRD. The different composition was confirmed by the much brighter appearance of these features in the back-scattered electron (BSE) images, consistent with a higher average atomic number expected for the latter phase. On the other hand, these particles were not visible in either the SE or the BSE images of Cu/mesoH-ZSM-5. Finally, some accessible mesopores appeared in the external surface of the hierarchical zeolite crystals, resulting from the post-synthetic modification.

TEM images of the fresh copper-loaded conventional zeolite (Fig. 5a), evidenced a heterogeneous dispersion of copper oxide, with particles of similar shape to those visible in the BSE images in addition to smaller-sized nanoparticles decorating the external surface of the zeolite. Thus, a wide particle size distribution ranging from 2 to 20 nm was attained. No significant differences were appreciated when this sample was used repeatedly as a HC trap in the CST (Fig. 5b). In the case of the copper-loaded hierarchical ZSM-5 (Fig. 5c), the TEM micrographs confirmed the preserved crystallinity of the zeolite. This alkaline treated and acid washed sample exhibits intracrystalline mesopores of about 10 nm diameter in agreement with the pore-size distribution determined by N_2 sorption. It is noteworthy that the large copper oxide particles identified for the conventional zeolite were less prominent in the hierarchical sample. In addition, as observed for the conventional zeolite, no differences in the dispersion of the copper oxide particles were noticed after use (Fig. 5d).

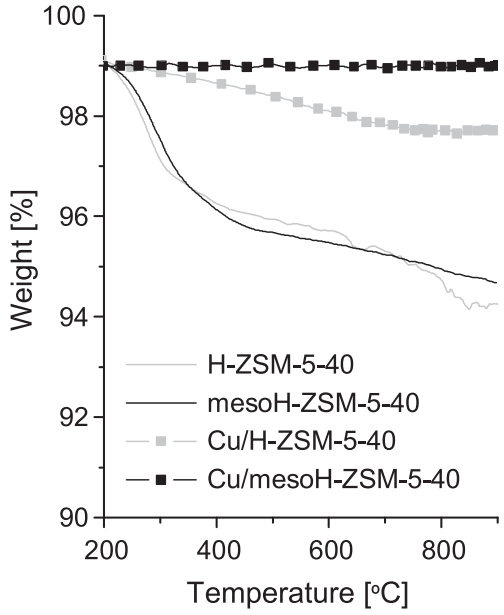

Fig. 3. TGA data of the used samples after three consecutive CSTs.

Fig. 6 shows the HAADF-STEM images of both the conventional and hierarchical zeolites loaded with copper. Consistent with the BSE images, the rod-like copper oxide structures appearing with brighter contrast were observed surrounding the conventional zeolite particles. The image of the hierarchical zeolite clearly highlighted the uniform distribution of intracrystalline mesopores. It is likely that small nanoparticles decorated the entire surface, but the tendency to sinter and to form large nanoparticles was strongly reduced by the larger spatial separation.

FTIR spectra in the hydroxyl stretching region of the different HC traps are reported in Fig. 7. Equivalent intensities of the band corresponding to bridging hydroxyls at Brønsted acid sites (3610 cm^{-1}), an increased intensity of the band arising from isolated terminal silanol groups (3740 cm^{-1}), and a decreased intensity of the broad contribution associated with silanol nests (centered at ca. 3450 cm^{-1}) compared with the conventional H-ZSM-5, were as expected for the hierarchical zeolite in protonic form [32]. In the Cu-loaded analogues, the interaction of copper with the related hydroxyl groups resulted in decreased band intensities. This was most noticeable for the Brønsted acid hydroxyls, which disappeared almost entirely, supporting the incorporation of copper in cation exchange sites [21,43]. As a consequence of the reduced intensity of the Brønsted hydroxyl stretch, the band at 3640 cm^{-1} appeared more prominently in the copper-containing zeolites. This frequency is associated with hydroxyls at defect sites within the zeolite structure, which clearly did not interact significantly with any copper species [44]. No significant changes were evidenced by FTIR following CST testing (Fig. 7).

Temperature-programmed desorption of ammonia (NH_3-TPD) was used to further characterize the strength of accessible acid sites in the catalysts (Fig. 8). Due to the conditions used, all the samples displayed a desorption peak below 150 °C related to weakly physisorbed ammonia. At higher temperatures, two characteristic contributions centered, at ca. 180 and 370 °C were similarly distinguished for the protonic zeolites, in agreement with the comparable acidic properties of the conventional and hierarchical H-ZSM-5 zeolites. A substantially different behavior was seen for the copper-containing zeolites, which exhibited additional desorption peaks (centered at ca. 280 and 460 °C), while the peaks related to the protonic zeolites became less noticeable. The creation of distinct adsorption sites in copper-containing ZSM-5 zeolites has been previously reported [45–49]. In particular, at high copper loadings, various copper species including isolated Cu^{2+} ions, $Cu^{2+}O^{-}$ and $Cu^{2+}O^{2-}Cu^{2+}$ compounds, and CuO clusters, can exist, and consequently the number and strength of sites are expected to depend on the content and location (e.g. specific cation exchange sites

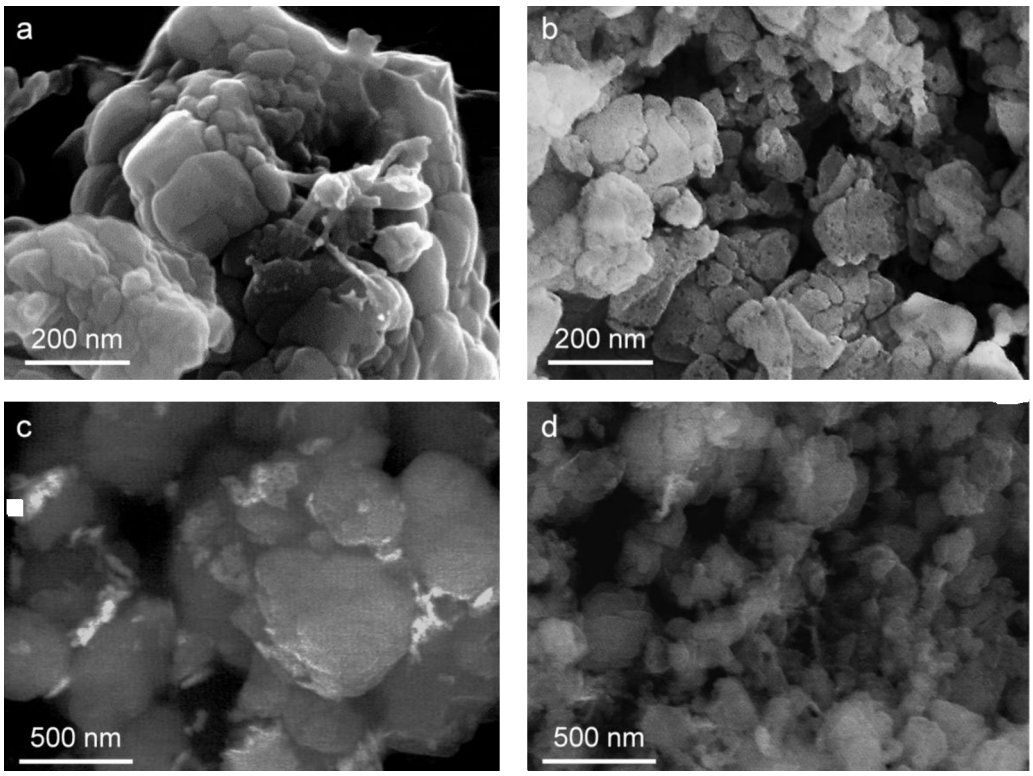

Fig. 4. Secondary (a and b) and back-scattered (c and d) electron images of Cu/H-ZSM-5 and Cu/mesoH-ZSM-5, respectively.

and extraframework) of the copper species. Furthermore, the findings of Il'ichev et al., who combined electron spin resonance with NH_3-TPD and evolved gas analysis, specifically related the higher temperature desorption peaks observed over copper-loaded ZSM-5 with adsorption complexes formed on Cu^{2+} ions, demonstrating that these sites caused the decomposition of ammonia to H_2O and N_2 [49]. In this case, the high-temperature contribution was greater for the hierarchical zeolite, evidencing a higher number of such strongly adsorbing sites in this sample. Cu/mesoH-ZSM-5 also appeared to have the largest interaction with ammonia molecules. In line with the FTIR observations, no significant change in the NH_3-TPD profiles was visible for the protonic zeolites after three consecutive CSTs. However, some differences were noticeable with respect to the high-temperature desorption peak for the copper-loaded zeolites, which disappeared completely in the microporous Cu/H-ZSM-5 sample. It is possible that these sites are blocked by the coke formation evidenced in this sample, or that the underlying copper species suffered from sintering, but in the latter case this does not appear to be related with dealumination of the zeolite framework. The fact that the high-temperature desorption peak remained in the case of Cu/mesoH-ZSM-5, evidenced the superior stability of the hierarchical sample.

3.2. Catalyst performance

Fig. 9 shows the CST profiles observed over the conventional and hierarchical acid zeolites. During the first minutes of the CST, the signal of HCs (propene and toluene) was kept close to zero in both cases, due to either physical adsorption or chemical interactions between the HCs and the adsorbent surface [19]. As the system temperature was increased, the adsorption was no longer favored and the CST profile showed HC evolution peaks, firstly for propene and, after for toluene. Eventually, the HC signals reached a maximum and started to decrease due to the onset of catalytic combustion above the HC desorption temperature, until reaching steady-state values. HC desorption was detected earlier over meso/H-ZSM-5 than H-ZSM-5 (see Figs. 9 and 10), and a higher concentration of propene and toluene was observed over the former zeolite at steady state. The lower adsorption capacity evidenced over the hierarchical zeolite in protonic form can be attributed to the reduced micropore volume of this sample (see Table 1), whereas the decreased retention of HCs could be related to the greater accessibility of the adsorption sites and consequently facilitated desorption of the trapped HCs with increasing temperature. It is important to note that by applying a constant feed gas composition during the CST, the location of the HC peak can be shifted to higher temperatures since, in addition to the temperature ramp, the desorption of HCs trapped by the zeolite also depends on the concentration gradient in the feed.

Limited catalytic activity was observed over the protonic zeolites, especially for mesoH-ZSM-5, which showed the lowest CO_2 evolution and the lowest propene desorption temperature of all the HC traps studied (see Figs. 10 and 11(a)). On the other hand, Fig. 9 shows the relative CST profiles measured for the copper-loaded counterparts. A clear reduction of the HC signals was observed at the reactor outlet over both Cu/H-ZSM-5 and Cu/mesoH-ZSM-5 compared to the base protonic zeolites, and even close to zero signals were obtained in the case of the hierarchical sample. The remarkably improved performance of both copper-containing zeolites is consistent with the enhanced interaction of HCs due to the presence of the stronger adsorption sites evidenced by NH_3-TPD. In terms of catalytic activity, although both solids were able to oxidize the HCs, the catalytic combustion started earlier in the hierarchical sample (Fig. 11a) in line with the better dispersion of copper nanoparticles observed for this sample. The oxidation of HC under lean conditions was also reported by Meng et al. [50], who observed ca. 70% toluene conversion at 400 °C over Mn-ZSM-5 catalysts. The reduced CO_2 emission over Cu/mesoH-ZSM-5 than over Cu/H-ZSM-5 at the end of the CST, is thought to result from the more efficient desorption of HCs at lower temperatures in the

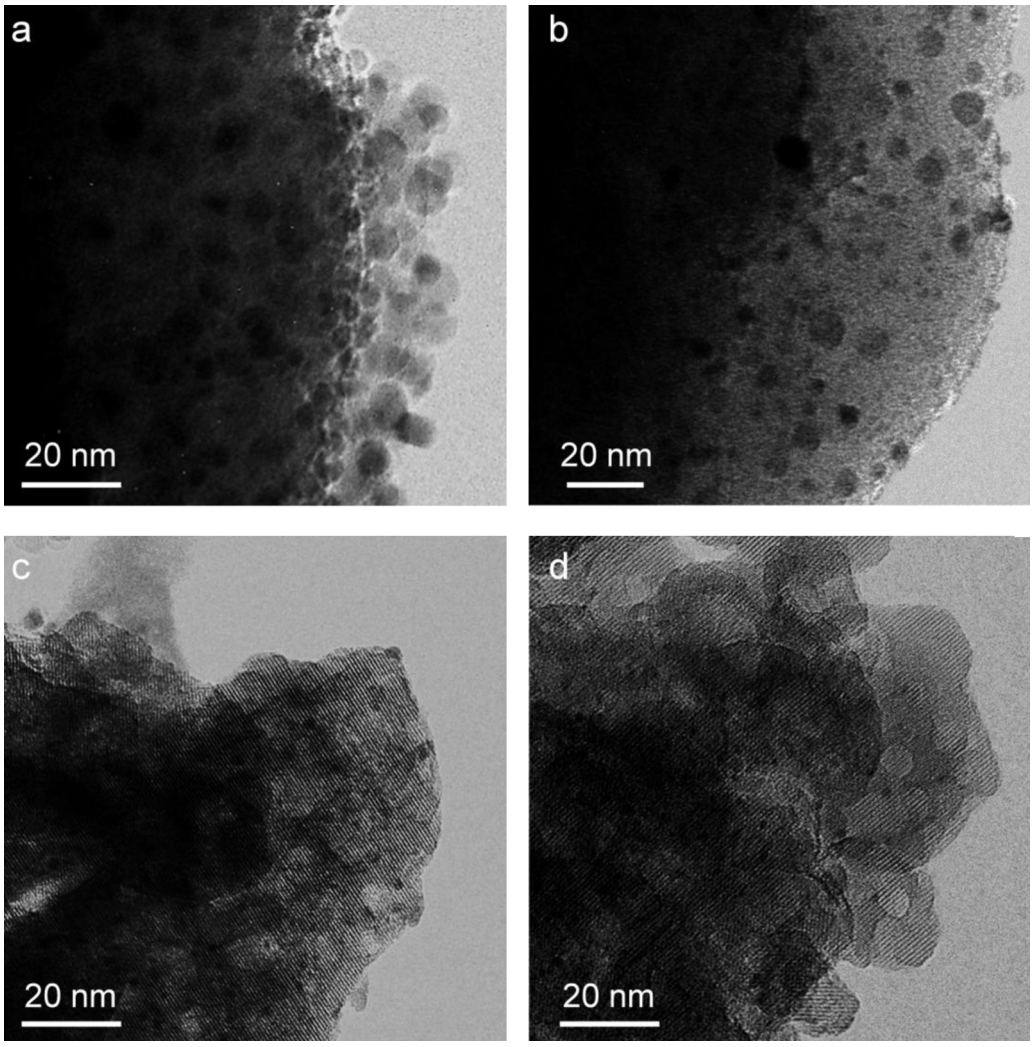

Fig. 5. TEM images of Cu/H-ZSM-5 (a and b) and Cu/mesoH-ZSM-5 (c and d), as-synthesized (a and c), and after three CST cycles (b and d), respectively.

former sample. Although a high trapping capacity is typically desired, in this case the faster desorption of HCs is countered by a more efficient catalytic combustion of the HCs desorbed.

The possible occurrence of propene polymerization over the samples was studied by mass spectrometric analysis of the evolved gas components, since any oligomers formed during the driving cycle could also be emitted to the atmosphere. As seen on

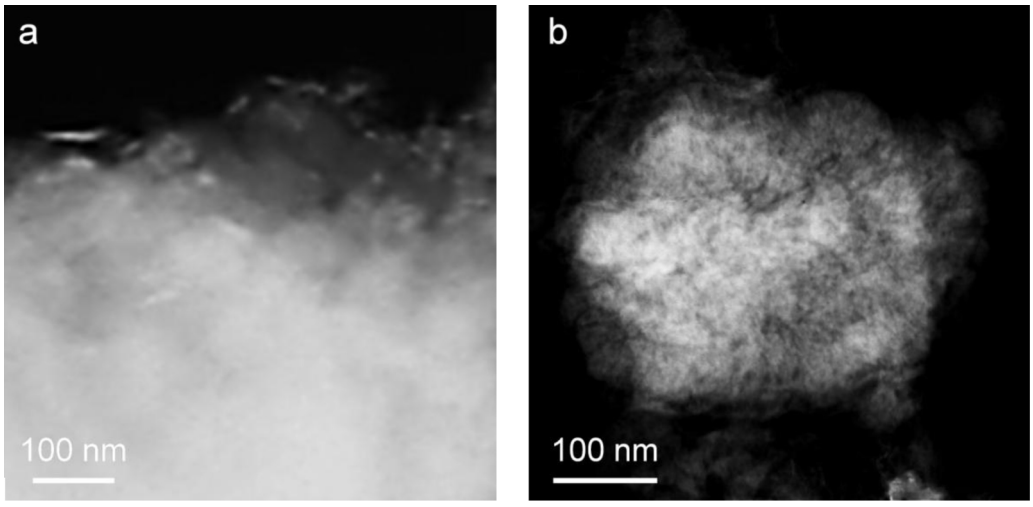

Fig. 6. HAADF-STEM images of Cu/H-ZSM-5 (a) and Cu/mesoH-ZSM-5 (b).

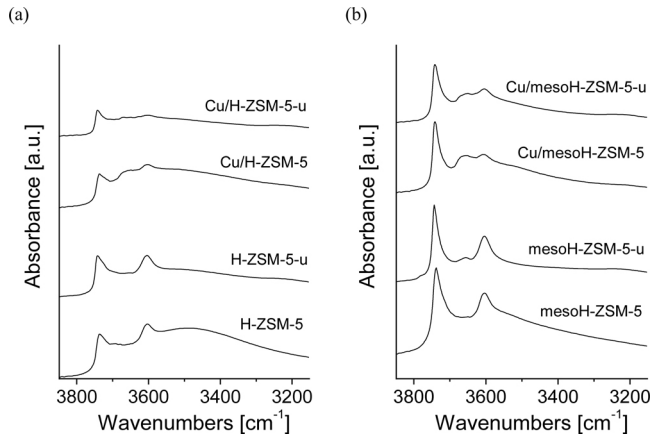

Fig. 7. FTIR spectra in the hydroxyl stretching region of the as-synthesized microporous (a) and hierarchical (b) HC traps, and following three CST cycles (designated-u).

comparison of the fragmentation patterns observed during the CST at 240 °C (Fig. 12), several m/z peaks could be observed in the range m/z = 20-100 over the protonic zeolites, of which a signal at m/z = 56 was one of the most prominent. The evolution of the peak was more prominent over the hierarchical zeolite than over the conventional counterpart, which could be attributed to a better accessibility to the acid sites where the production of these compounds takes place (Fig. 11b). In contrast to the extensive oligomerization observed over the zeolites in protonic form, the introduction of copper seemed to completely inhibit the emission and/or formation of these molecules for which no mass fragments were detected (see Fig. 12).

Moreover, it is noted that both acid zeolites and the microporous Cu/H-ZSM-5 catalyst deactivated slightly after three CSTs (see Fig. 10). TGA analysis revealed the presence of coke (ca. 1,1 wt%) in this sample (see Fig. 3). On the other hand, no deactivation was observed for the hierarchical copper-exchanged zeolite after three consecutive cycles (neither propene emission nor coke formation was detected).

Finally, in order to assess the performance of the copper-loaded hierarchical zeolite under a wider range of operational conditions, two additional scenarios have been considered. In the first case, the amount of oxygen in the main stream was decreased to 0,115% (v/v). This would correspond to the stoichiometric oxygen required to control the current HC emissions. The propene desorption temperature of both copper-loaded zeolites after 4 CSTs are shown

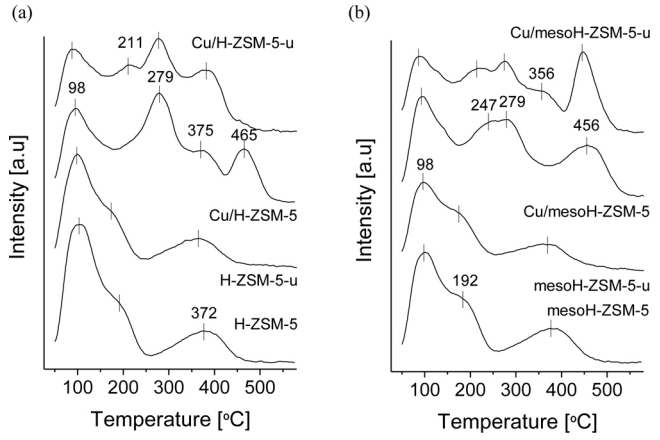

Fig. 8. NH_3-TPD profiles of the as-synthesized microporous (a) and hierarchical (b) HC traps, and following three CST cycles (designated-u).

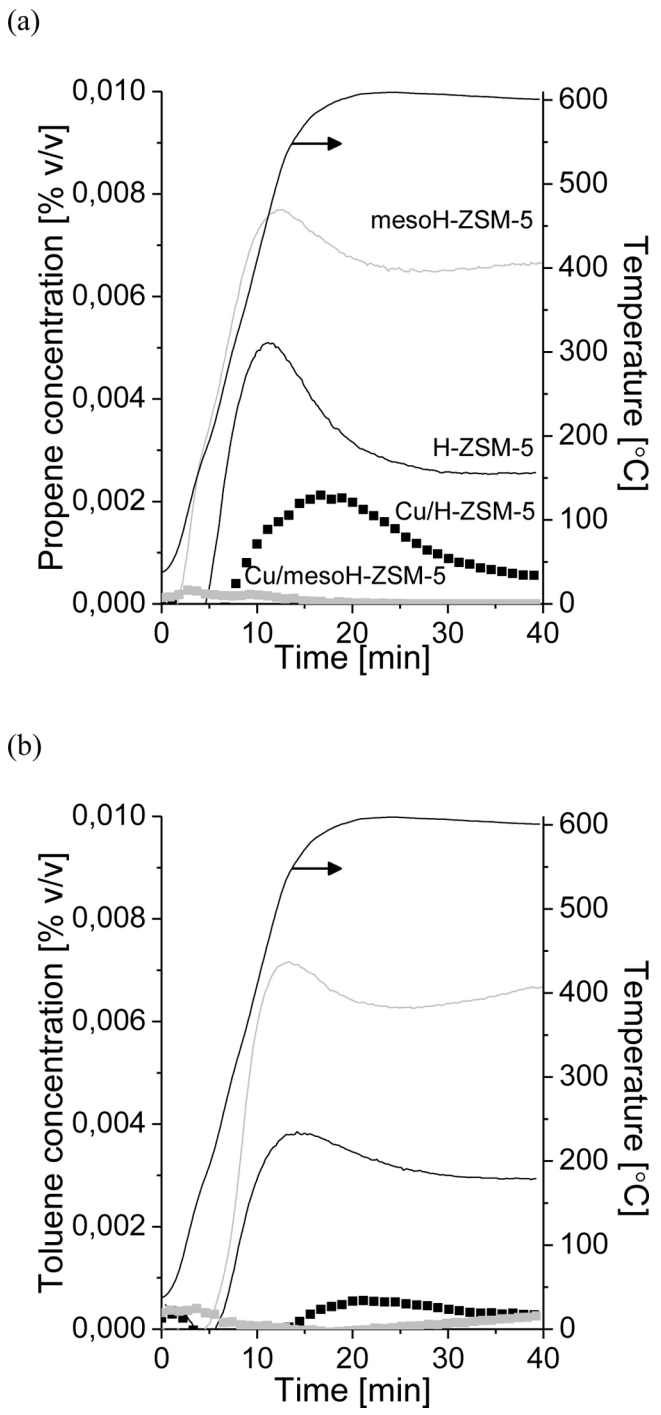

Fig. 9. Simulated CSTs for conventional (black lines) and hierarchical (grey lines) zeolites, propene (a), toluene (b). Conditions: 0,01% (v/v) propene, 0,0087% (v/v) toluene, 1% (v/v) O_2, 10% (v/v) H_2O and Ar balance, GHSV = 60 K h^{-1}.

in Fig. 13. As noted, the propene desorption temperature of the microporous sample is lower than that observed for the hierarchical counterpart, which could be attributed to the improved catalytic activity demonstrated by the latter. Encouragingly, efficiencies higher than 90% were achieved in both cases. Under these conditions, TGA analysis evidenced only marginal coke formation after 4 cycles, which agrees well with the stability of the traps under these conditions.

In the second case, 16% CO (v/v), was introduced in the main gas stream, corresponding to a lambda value (the ratio of the actual air-fuel ratio to the stoichiometric air-fuel ratio) of ca. 1. Under

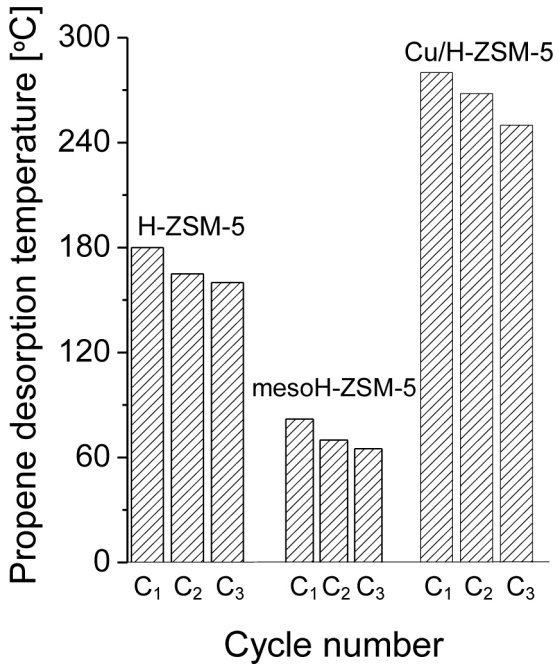

Fig. 10. Propene desorption temperature for different HC traps for the three CSTs. C_1, C_2 and C_3 denote 1st, 2nd, and 3rd cycle, respectively. Conditions: 001% (v/v) propene, 0,0087% (v/v) toluene, 1% (v/v) O_2, 10% (v/v) H_2O and Ar balance, GHSV = 60 K h^{-1}. No results are shown for the copper-loaded hierarchical zeolite since no propene desorption was observed for this sample.

these circumstances, both CO and the HC would compete for the oxygen in the exhaust stream. The propene desorption temperatures of the Cu-loaded zeolites after 4 CSTs are shown in Fig. 13. As can be observed, the performance of the traps slightly declines compared to that exhibited in the absence of CO (see Fig. 10). The low propene desorption temperature observed for the microporous zeolite (below 175 °C) could be ascribed to the inferior catalytic activity of this sample. In contrast, the retention of propene to temperatures higher than 290 °C and the overall propene efficiency of greater than 97% evidenced for the copper-loaded hierarchical zeolite are promising results. Unfortunately, a slight deactivation was observed in both cases. TGA analysis revealed the presence of a similar amount of coke (7 wt%) in both samples after 4 cycles, which could be one reason for the reduced propene efficiency. Accordingly, a very active CO oxidation catalyst prior to the trap could be necessary to diminish the deactivation phenomenon.

4. Discussion

In a previous work [19], it was observed that an optimum partially copper-exchanged zeolite could behave as an ideal trap under simulated cold-start conditions at a GHSV of 10 K h^{-1}. The amount of copper in ion-exchange positions and the presence of CuO particles on the external surface of the zeolite crystals were found to be key parameters for the performance of these solids as HC traps. None of the materials studied, however, were able to trap all HCs upon increasing the GHSV from 10 up to 60 K h^{-1}. Clearly, an optimal interplay between the accessibility to copper in ion-exchanged positions (beneficial for the sorption process) and copper as CuO particles (beneficial for the combustion of the desorbed HCs [51]) should be achieved. Now, in order to overcome these restrictions, alkaline treatment combined with a sequential acid wash was applied to the commercial H-ZSM-5 zeolite. The result was a hierarchical zeolite that had an ideal behavior as a HC trap at higher GHSV. A larger external surface, arising from the introduction of intracrystalline mesopores, coupled with the preserved intrinsic

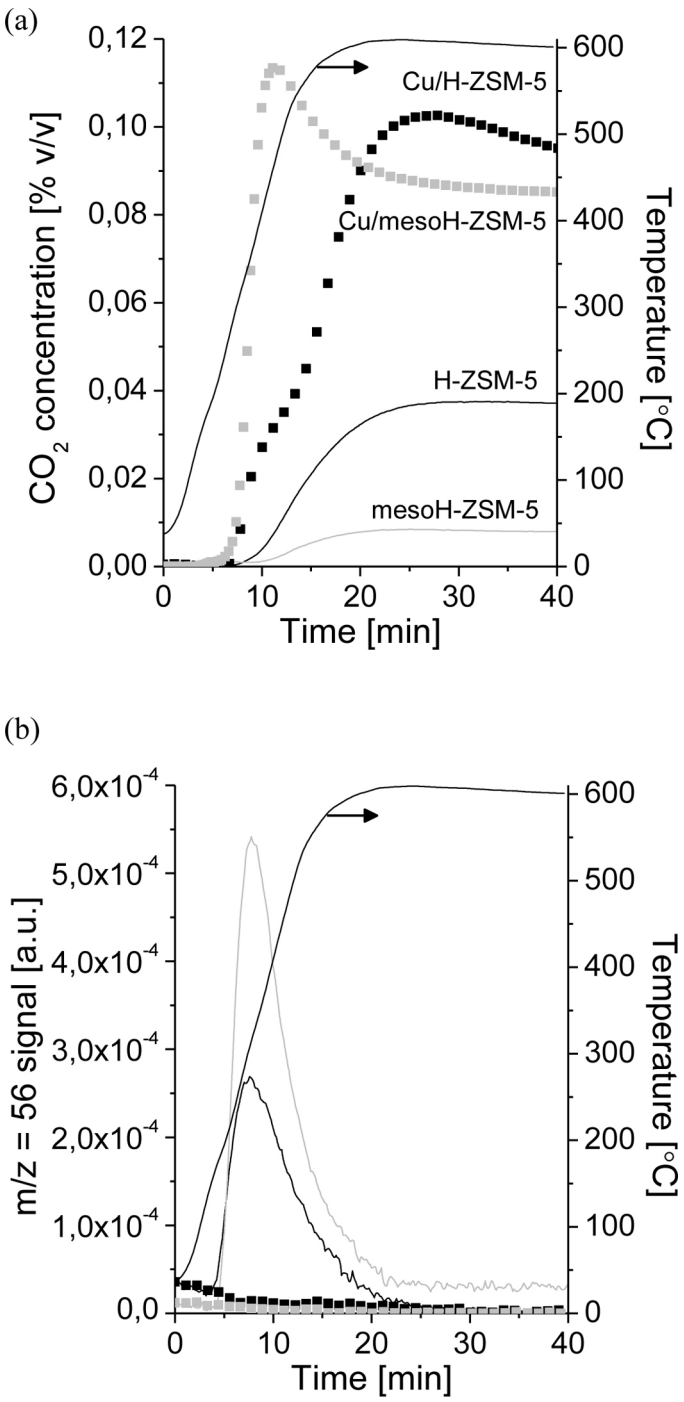

Fig. 11. CO_2 (a) and oligomer (b) evolution during the simulated CSTs for different HC traps. Conditions: 0.01% (v/v) propene, 0.0087% (v/v) toluene, 1% (v/v) O_2, 10% (v/v) H_2O and Ar balance, GHSV = 60 K h^{-1}.

crystallinity and acidic properties of the conventional H-ZSM-5, led to an enhanced accessibility of copper sites located in ion-exchanged positions and to an increased dispersion of oxidic copper species. Based on the FTIR results, high degrees of ion exchange were achieved in both the conventional and hierarchical sample. Nevertheless, the copper-loaded hierarchical sample exhibited the highest catalytic activity for HC combustion. According to the analysis by XRD, FEG-SEM, and HAADF-STEM, the conventional sample presented larger copper oxide particles with rod-like crystal morphology visible on the external surface of zeolite particles, which were less prominent in the hierarchical analogue. This

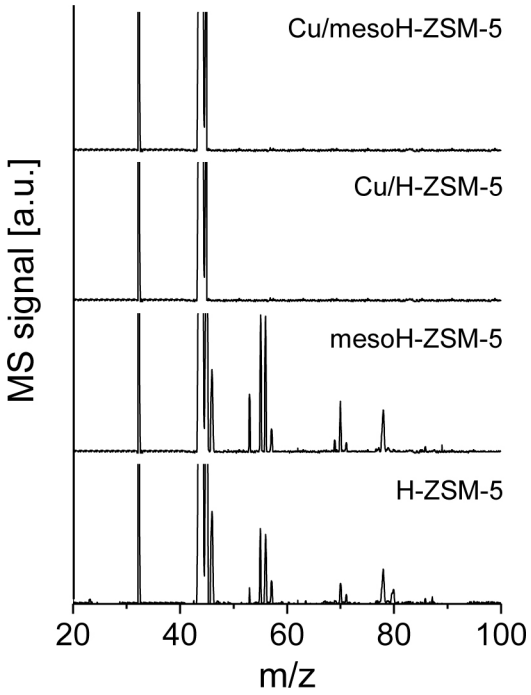

Fig. 12. Mass scan in the range m/z = 20–100 during the CST for different HC traps. Conditions: 0,01% (v/v) propene, 0,0087% (v/v) toluene, 1% (v/v) O_2, 10% (v/v) H_2O and Ar balance, GHSV = 60 K h^{-1}, T = 240 °C.

confirms that an improved dispersion of copper oxide nanoparticles was achieved due to the increased external surface of the hierarchical zeolite. Consequently, the copper-loaded hierarchical zeolite showed the lowest propene desorption temperature, complete removal of oligomers, no coke formation, and almost full HC conversion at high temperature. Finally, a higher stability was evidenced for the hierarchical copper-loaded zeolite, which exhibited no signs of deactivation after three consecutive cycles under very demanding operational conditions, while minor deactivation was noted over the conventional copper-loaded zeolite. This is consistent with the decreased concentration of high-strength

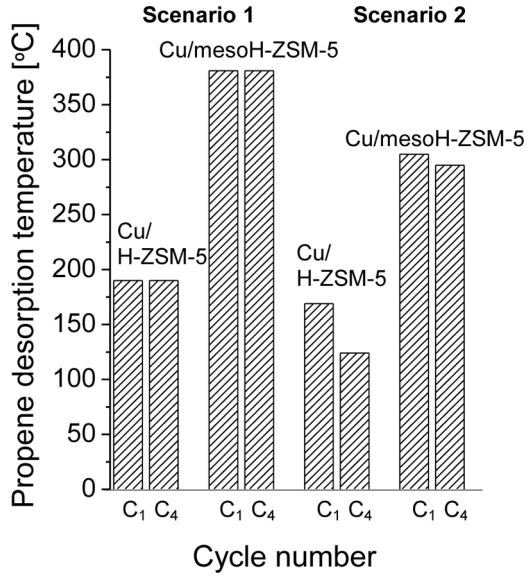

Fig. 13. Propene desorption temperature for different HC traps for the two scenarios. C_1 and C_4 denote 1st and 4th cycle, respectively. Conditions scenario 1: 0,01% (v/v) propene, 0,0087% (v/v) toluene, 0,115% (v/v) O_2, 10% (v/v) H_2O and Ar balance, GHSV = 60 K h^{-1}; Conditions scenario 2: 0,01% (v/v) propene, 0,0087% (v/v) toluene, 1% (v/v) O_2, 1,6% (v/v) CO, 10% (v/v) H_2O and Ar balance, GHSV = 60 K h^{-1}.

adsorption sites and the presence of coke evidenced for the latter sample by NH_3-TPD and TGA analysis, respectively. Thus, both blockage of the adsorption or catalytic sites due to coke formation, or their loss due to the migration of copper species could originate the deactivation observed in this case, although the occurrence of sintering could not be confirmed by XRD or TEM. The high stability of the copper loaded hierarchical zeolite is in agreement with previous findings [30], where it was suggested that the sintering of cobalt catalysts could be suppressed when supported on hierarchical zeolites.

Conversely, although no deactivation has been observed for the copper-loaded hierarchical zeolite, this sample was tested under much more highly demanding operational conditions, i.e. (i) with a stoichiometric oxygen concentration and (ii) in the presence of CO. The results are still encouraging since HC removal efficiencies greater than 90% are achieved, despite the observation of a slight deactivation when CO is present in the main gas flow. Under these conditions, appreciable amounts of coke are deposited on the HC trap surface, which is a well-known problem observed for this type of materials when applied for NO_x abatement that could possibly be diminish by using a very active CO oxidation catalyst prior to the trap. Consequently, a higher number of cycles under real conditions should be performed in order to ensure the promising HC removal efficiency observed for this material. In addition to this, joint studies on the optimum configuration of the HC trap and the TWC in the gas exhaust manifold with respect to the operating regime and consequent stability need to be undertaken.

5. Conclusions

This study revealed that the development of mesopores by alkaline treatment prior to the introduction of copper enhanced the catalytic trapping performance of Cu/H-ZSM-5 zeolites. Results of simulated CSTs showed that the increased external surface area played an important role in the properties of the hierarchical material. These structural features translated into a stable bifunctional catalyst that was able to perform as an ideal trap under very demanding operational conditions, GHSV: 60 K h^{-1}. The hierarchical copper-loaded zeolite maintained its remarkable HC adsorption capacity, while a better dispersion of copper nanoparticles on the zeolite external surface led to exceptional catalytic properties over multiple consecutive cycles. Although high efficiencies were reached for this material, slight deactivation was evidenced over the copper-loaded hierarchical zeolite under very demanding operational conditions. Thus, a higher number of cycles under a wider range of feed compositions, such as in the presence of other hydrocarbons or CO, are necessary to confirm the potential application of these materials for HC removal under cold start conditions.

Acknowledgements

The authors would like to thank to MINECO and FEDER funds for providing support for this work (Project CTQ2012-37984-C02-01). The authors would also like to thank to Ministry de Ciencia e Innovación - CSIC for partial support (Project 201080I031). B.P. thanks the Spanish Ministry of Education (FPU grant AP2009-3544). S.M. and J.P.R. acknowledge the Swiss National Science Foundation (Project 200021-134572 and ScopeM of the Swiss Federal Institute of Technology ETHZ).

References

[1] G.N. Pontikakis, G.S. Konstantas, A.M. Stamatelos, J. Eng. Gas Turb. Power 126 (2004) 906–923.
[2] S.-M. Choi, Y.-K. Youn, C.-B. In, G.-K. Yeo, SAE Technical Paper Series, 2006-01-0850, 2006.

[3] J. Park, S.J. Park, I. Nam, G.K. Yeo, J.K. Kil, Y.K. Youn, Microporous Mesoporous Mater. 101 (2007) 264–270.
[4] G.C. Koltsakis, A.M. Stamatelos, Prog. Energy Combust. Sci. 23 (1997) 1–39.
[5] D.S. Lafyatis, G.P. Ansell, S.C. Bennett, J.C. Frost, P.J. Millington, R.R. Rajaram, A.P. Walker, T.H. Ballinger, Appl. Catal. B 18 (1998) 123–135.
[6] A. Iliyas, M.H. Zahedi-Niaki, M. Eić, S. Kaliaguine, Microporous Mesoporous Mater. 102 (2007) 171–177.
[7] K.F. Czaplewski, T.L. Reitz, Y.J. Kim, R.Q. Snurr, Microporous Mesoporous Mater. 56 (2002) 55–64.
[8] N.R. Burke, D.L. Trimm, R.F. Howe, Appl. Catal. B 46 (2003) 97–104.
[9] S.P. Elangovan, M. Ogura, M.E. Davis, T.J. Okubo, Phys. Chem. B 108 (2004) 13059–13061.
[10] H.W. Jen, K. Otto, Catal. Lett. 26 (1994) 217–225.
[11] J.M. López, M.V. Navarro, T. García, R. Murillo, A.M. Mastral, F.J. Varela-Gandía, D. Lozano-Castelló, A. Bueno-López, D. Cazorla-Amorós, Microporous Mesoporous Mater. 130 (2010) 239–247.
[12] V. Golubeva, A. Korableva, O. Anischenko, A. Nemova, N. Yegorushina, L. Kustov, G. Kapustin, U.S. Rohatgi, World Acad. Sci. Eng. Technol. 55 (2011) 7–26.
[13] R. Yoshimoto, K. Hara, K. Okumura, N. Katada, M. Niwa, J. Phys. Chem. C 111 (2007) 1474–1479.
[14] R.M. Serra, E.E. Miró, P. Bolcatto, A.V. Boix, Microporous Mesoporous Mater. 147 (2012) 17–29.
[15] J.-H. Park, S.J. Park, H.A. Ahn, I.-S. Nama, G.K. Yeo, J.K. Kil, Y.K. Youn, Microporous Mesoporous Mater. 117 (2009) 178–184.
[16] K. Mukai, H. Kanesaka, H. Akama, T. Ikeda, SAE Technical Paper Series, 2004-01-2983, 2004.
[17] H.-X. Li, J.M. Donohue, W.E. Cormier, Y.F. Chu, Stud. Surf. Sci. Catal. 158 (2005) 1375–1382.
[18] B. Puértolas, M. Navlani-García, J.M. López, T. García, R. Murillo, A.M. Mastral, M.V. Navarro, D. Lozano-Castelló, A. Bueno-López, D. Cazorla-Amorós, Chem. Commun. 48 (2012) 6571–6573.
[19] M. Navlani-García, B. Puértolas, D. Lozano-Castelló, D. Cazorla-Amorós, M.V. Navarro, T. García, Environ. Sci. Technol. 47 (2013) 5851–5857.
[20] C. Torre-Abreu, M.F. Ribeiro, C. Henriques, F.R. Ribeiro, G. Delahay, Catal. Lett. 43 (1997) 31–36.
[21] S. Vergne, A. Berreghis, J. Tantet, C. Canaff, P. Magnoux, M. Guisnet, N. Davias, R. Noirot, Appl. Catal. B 18 (1998) 37–50.
[22] I.C. Hwang, D.H. Kim, S.I. Woo, Catal. Today 44 (1998) 47–55.
[23] F. Seyedeyn-Azad, D.-K. Zhang, Catal. Today 68 (2001) 161–171.
[24] D.W. Fickel, E.D. Addio, J.A. Lauterbach, R.F. Lobo, Appl. Catal. B 102 (2011) 441–448.
[25] V. Houel, D. James, P. Millington, S. Pollington, S. Poulston, R. Rajaram, R. Torbati, J. Catal. 230 (2005) 150–157.
[26] Y. Zhang, M. Flytzani-Stephanopoulos, J. Catal. 164 (1996) 131–145.
[27] J.C. Groen, L.A.A. Peffer, J.A. Moulijn, J. Pérez-Ramírez, Colloids Surf. 241 (2004) 53–58.
[28] J. Pérez-Ramírez, C.H. Christensen, K. Egeblad, C.H. Christensen, J.C. Groen, Chem. Soc. Rev. 37 (2008) 2530–2542.
[29] D. Verboekend, J. Pérez-Ramírez, Catal. Sci. Technol. 1 (2011) 879–890.
[30] S. Sartipi, J.E. van Dijk, J. Gascon, F. Kapteijn, Appl. Catal. A 456 (2013) 11–22.
[31] J.T. Kummer, Prog. Energy Comb. Sci. 6 (1980) 177–199.
[32] D. Verboekend, M. Milina, S. Mitchell, J.C. Groen, J. Pérez-Ramírez, J. Phys. Chem. C 115 (2011) 14193–14203.
[33] P.N. Botsaris, D. Bechrakis, P.D. Sparis, Appl. Catal. A 243 (2003) 285–292.
[34] R.M. Heck, R.J. Farrauto, Appl. Catal. A 221 (2001) 443–457.
[35] V.A. Chakravarthy, J.C. Conklin, C.S. Daw, E.F. D'Azevedo, Appl. Catal. A 241 (2003) 289–306.
[36] C.M.L. Scholz, PhD Dissertation, Technische Universiteit Eindhoven, 2007.
[37] K.S. MacCartney, Catalytic converter tests, 2010.
[38] P. Yarlagadda, C.R.F. Lund, E. Ruckenstein, Appl. Catal. 62 (1990) 125–139.
[39] T.J. Gricus Kofke, R.J. Gorte, J. Catal. 115 (1989) 233–243.
[40] International zeolite association website: http://www.iza-online.org/, Accessed on September 2013.
[41] P. Ciambelli, P. Corbo, M. Gambino, G. Minelli, G. Moretti, P. Porta, Catal. Today 26 (1995) 33–39.
[42] J.C. Groen, J.C. Jansen, J.C. Moulijn, J. Pérez-Ramírez, J. Phys. Chem. B 108 (2004) 13062–13065.
[43] A.V. Ivanov, G.W. Graham, M. Shelef, Appl. Catal. B 21 (1999) 243–258.
[44] C.L. Angell, P.C. Schaffer, J. Phys. Chem. 69 (1965) 3463–3470.
[45] N.A.S. Amin, D.D. Anggoro, J. Nat. Gas Chem. 12 (2003) 123–134.
[46] M.Y. Kustova, S.B. Rasmussen, A.L. Kustov, C.H. Christensen, Appl. Catal. B 67 (2006) 60–67.
[47] A. Sultana, T. Nanba, M. Haneda, M. Sasaki, H. Hamada, Appl. Catal. B 101 (2012) 61–67.
[48] S. Kieger, G. Delahay, B. Coq, B. Neveu, J. Catal. 183 (1999) 267–280.
[49] A.N. Il'ichev, V.A. Matyshak, V.N. Korchak, Y.B. Yan, Kinet. Catal. 42 (2001) 97–103.
[50] Y. Meng, H.C. Genuino, C.-H. Kuo, H. Huang, S.-Y. Chen, L. Zhang, A. Rossi, S.L. Suib, J. Am. Chem. Soc. 135 (2013) 8594–8605.
[51] E. Finocchio, R.J. Willey, G. Busca, V. Lorenzelli, J. Chem. Soc., Faraday Trans. 93 (1997) 175–180.